Dynamics of "internal" interannual variability of the Indian summer monsoon in a GCM

B. N. Goswami and Prince K. Xavier

Centre for Atmospheric and Oceanic Sciences, Indian Institute of Science, Bangalore, India

Received 4 April 2005; revised 20 July 2005; accepted 1 September 2005; published 20 December 2005.

[1] The poor predictability of the Indian summer monsoon (ISM) appears to be due to the fact that a large fraction of interannual variability (IAV) is governed by unpredictable ''internal'' low frequency variations. Mechanisms responsible for the internal IAV of the monsoon have not been clearly identified. Here, an attempt has been made to gain insight regarding the origin of internal IAV of the seasonal (June–September, JJAS) mean rainfall from ''internal'' IAV of the ISM simulated by an atmospheric general circulation model (AGCM) driven by fixed annual cycle of sea surface temperature (SST). The underlying hypothesis that monsoon ISOs are responsible for internal IAV of the ISM is tested. The spatial and temporal characteristics of simulated summer intraseasonal oscillations (ISOs) are found to be in good agreement with those observed. A long integration with the AGCM forced with observed SST, shows that ISO activity over the Asian monsoon region is not modulated by the observed SST variations. The internal IAV of ISM, therefore, appears to be decoupled from external IAV. Hence, insight gained from this study may be useful in understanding the observed internal IAV of ISM. The spatial structure of the ISOs has a significant projection on the spatial structure of the seasonal mean and a common spatial mode governs both intraseasonal and interannual variability. Statistical average of ISO anomalies over the season (seasonal ISO bias) strengthens or weakens the seasonal mean. It is shown that interannual anomalies of seasonal mean are closely related to the seasonal mean of intraseasonal anomalies and explain about 50% of the IAV of the seasonal mean. The seasonal mean ISO bias arises partly due to the broad-band nature of the ISO spectrum allowing the time series to be aperiodic over the season and partly due to a non-linear process where the amplitude of ISO activity is proportional to the seasonal bias of ISO anomalies. The later relation is a manifestation of the binomial character of rainfall time series. The remaining 50% of the IAV may arise due to land-surface processes, interaction between high frequency variability and ISOs, etc.

Citation: Goswami, B. N., and P. K. Xavier (2005), Dynamics of ''internal'' interannual variability of the Indian summer monsoon in a GCM, *J. Geophys. Res.*, *110*, D24104, doi:10.1029/2005JD006042.

1. Introduction

[2] With a large fraction of world population depending on the monsoon rainfall, prediction of summer monsoon rainfall at least one season in advance assumes great significance. For over a century, attempts have been made to predict seasonal mean monsoon rainfall using empirical techniques involving local and global antecedent parameters that correlate with the monsoon rainfall [*Blanford*, 1884; *Walker*, 1923, 1924; *Gowarikar et al.*, 1989; *Sahai et al.*, 2003]. The linear and non-linear regression models as well as the neural network based models [e.g., *Goswami and Srividya*, 1996] perform reasonably well when the monsoon is close to normal but fails to predict the extremes with useful skill. A case in point is the failure of almost all empirical models in predicting the 2002 drought. Another intrinsic limitation of the empirical techniques arises from interdecadal variation of the correlations between predictors and monsoon rainfall [*Kriplani and Kulkarni*, 1997; *Kumar et al.*, 1999; *Krishnamurthy and Goswami*, 2000]. Dynamical prediction of the seasonal mean monsoon using state of the art climate models, therefore, offers a logical alternative to empirical forecasting. Unfortunately, the skill of prediction of the summer precipitation over the Asian monsoon region is currently negligible for almost all state of the art atmospheric general circulation models (AGCM) [e.g., *Kang et al.*, 2004]. Multi-model super-ensemble forecasting [*Krishnamurti et al.*, 1999, 2000, 2001] shows some promise of improving the dynamical forecasts beyond the skill of individual models. Even the state of the art coupled GCMs presently have no useful skill in predicting the seasonal mean Indian summer monsoon (ISM) [*Krishnamurti et al.*, 2002; *Palmer et al.*, 2004].

[3] The inability of the state of the art AGCMs in predicting the seasonal mean monsoon appears to be due

0148-0227/05/2005JD006042$09.00

to three major factors. Firstly, even though AGCMs have improved over the last three decades in simulating the global climate in general, most models still have major systematic bias in simulating the seasonal mean ISM precipitation and its interannual variability [*Sperber and Palmer*, 1996; *Saji and Goswami*, 1997; *Gadgil and Sajani*, 1998; *Kang et al.*, 2002; *Wang et al.*, 2004]. Secondly, a part of IAV of the ISM arise from local interaction between the warm pool over the eastern Indian Ocean (IO), Bay of Bengal and western Pacific and the atmosphere [*Wang et al.*, 2003]. This air-sea interaction leads to a negative correlation between SST and precipitation over the region while AGCMs forced with observed SST tend to simulate a positive correlation between precipitation and SST. Therefore, coupled GCMs (CGCMs) are essential for predicting the IAV of the ISM. However, the current CGCMs also have large systematic biases in simulating the ISM limiting their utility for predicting the seasonal mean ISM. Finally, there appears to be an intrinsic limit on predictability of ISM due to the existence of significant 'climate noise' in this region. Following the seminal work of *Charney and Shukla* [1981], even though it has been shown [*Shukla and Wallace*, 1983; *Lau*, 1985; *Kumar and Hoerling*, 1995; *Shukla*, 1998; *Anderson et al.*, 1999; *Fennessy and Shukla*, 1999] that the tropical climate is largely driven by anomalous boundary conditions (ABC) and its simulation is much less sensitive to initial conditions, the ISM seems to be an exception within the tropics and its simulation seems to be quite sensitive to initial conditions [*Sperber and Palmer*, 1996; *Sperber et al.*, 2000; *Krishnamurthy and Shukla*, 2000; *Cherchi and Navarra*, 2003]. The sensitivity of simulation of ISM to initial conditions is associated with the existence of 'climate noise' or ''internal IAV'' over the region.

[4] The interannual variability of the tropical climate is partially governed by internally generated low frequency (LF) oscillations in addition to being forced by slowly varying ABC (such as the sea surface temperature, soil moisture, sea ice etc) arising from slow processes in the coupled ocean-atmosphere system. The internal LF variability in the atmosphere could, in principle, be generated through non-linear scale interactions between high frequency oscillations, non-linear interaction between intraseasonal oscillations (ISOs) and the seasonal cycle, interactions between flow and topography, feedback between organized convection and large scale dynamics etc. Estimates using AGCMs as well as observations indicate that a large fraction of IAV of the ISM is of internal origin and hence unpredictable. *Goswami* [1998] made an estimate of contributions from the two components to the IAV in the tropics using the GFDL AGCM and found that as large as 50% of the model's monsoon IAV could be governed by the internal component. In a recent study, *Kang et al.* [2004] using a different model came up with a similar estimate of contribution of the internal variability to the IAV over the Asian monsoon region. Using long daily observations, *Ajayamohan and Goswami* [2003] show that for both monthly mean as well as seasonal mean summer monsoon climate about 50% of the observed variability is governed by internal processes. These studies also show that there are certain regions in the tropics, such as central and eastern equatorial Pacific, central equatorial Atlantic etc., where contribution of internal variability is small and interannual variability is largely governed by external boundary forcing. These are regions where GCM simulations of seasonal mean show little sensitivity to initial conditions [e.g., *Shukla*, 1998] and where monthly and seasonal mean climate have high predictability.

[5] A clear understanding of mechanisms responsible for the internal IAV is imperative for making progress in seasonal monsoon prediction. However, this problem has not been addressed adequately so far. Several studies have provided circumstantial evidence of connection between monsoon ISOs and total IAV. Indian summer monsoon is known to have vigorous ISOs [*Yasunari*, 1979, 1980; *Sikka and Gadgil*, 1980; *Krishnamurti and Bhalme*, 1976; *Krishnamurti and Subrahmanyam*, 1982; *Goswami*, 2005] having time scales between 10 and 90 days that arise essentially due to internal dynamics of the atmosphere. *Fennessy and Shukla* [1994] and *Ferranti et al.* [1997] show similarity between spatial structure of ISO and IAV of the seasonal mean in models. *Goswami* [1994] speculated that interannual variations of statistics of monsoon ISO (such as preferred periodicity or frequency of occurrence etc.) could give rise to interannual variability of the seasonal mean. *Palmer* [1994] proposed a paradigm in which frequency of occurrence of chaotic ISO could result in interannual variability of the seasonal mean. Using long records of daily circulation and convection data, *Goswami and Ajayamohan* [2001] showed that the intraseasonal and interannual variability of the summer monsoon are governed by a common mode of spatial variability. They further showed that strong (weak) monsoon is characterized by higher probability of occurrence of active (break) conditions. *Sperber et al.* [2000] also showed that the ISO and IAV of monsoon are governed by a common spatial mode of variability and frequency of occurrence of the ISO could influence the seasonal mean and its IAV. While the studies just mentioned establish that frequency of occurrence of ISO and IAV of monsoon are related, a part of frequency change of ISO could arise due to regime changes in boundary forced climate. Mechanism for the internal component of the LF variability could not be clearly identified from these studies.

[6] The observed internal IAV of the ISM is a result of the coupled ocean-atmosphere interaction. Hence, a CGCM should ideally be employed to study mechanism responsible for observed internal IAV of the ISM. However, large systematic bias of current CGCMs in simulating the ISM may make such a study not very useful. Further, the atmosphere is the primary source of the high frequency variability in the coupled system. Therefore, the internal IAV is likely to be contributed largely by the atmosphere that may be modified to some extent by coupling with ocean. Hence, it is desirable to understand first, how the atmosphere generates internal IAV. The objective of the present study is to attempt to unravel mechanism(s) for internal IAV of the ISM generated by an atmosphere. For this purpose we choose a GCM and force the model with observed monthly SST to make sure that the model has a reasonable monsoon climatology and interannual variability compared to the observations. Then we integrate the model for a reasonably long period with no external interannual forcing. If the amplitude of the simulated IAV of Indian

monsoon is significant and/or its spatial structure bear some similarity to that of the observed IAV, the model simulations could provide insight regarding the origin of internal variability of the Indian summer monsoon. The model simulations are analyzed to test a hypothesis that monsoon ISOs are responsible for the internal IAV of the monsoon. The ISOs could influence the seasonal mean and its IAV through the following physical processes. If the spatial structure of the ISO mode has significant projection on that of the seasonal mean and if the probability density function of the ISOs is non-Gaussian, statistical average of ISO anomalies over the season (seasonal ISO bias) could lead to strengthening or weakening of the seasonal mean. A notable character of the rainfall anomalies is that they have a skewed probability distribution similar to the binomial distribution. For such a distribution, the second moment (variance) is proportional to the first (mean). Even the ISO anomalies of precipitation retain the binomial behavior to a large extent. Hence the ISO amplitude is proportional to the seasonal mean of ISO anomalies. The seasonal ISO bias, thus generated through this non-linear process also add to the IAV of the seasonal mean through the process discussed above. Evidence of supporting the mechanisms will be examined in the model simulations. The model experiment and data used for verification are described in section 2. The model climatology is discussed in section 3 and simulated IAV of Indian summer monsoon is discussed in section 4. The nature of the simulated monsoon ISO is described in section 5 while relationship between ISO and IAV of simulated monsoon is discussed in section 6. Results are summarized in section 7.

2. Model Experiments and Data

[7] The standard version of Community Climate Model version 3 (CCM3) [*Kiehl et al.*, 1998] developed by National Centre for Atmospheric Research (NCAR) is used in this study. It is a global spectral GCM with T42 horizontal resolution ($\approx 2.8^\circ \times 2.8^\circ$ Gaussian grid) and 18 levels in the vertical with top of the model at 4.8 hPa. Deep convection is simulated by the mass flux scheme of *Zhang and McFarlane* [1995] and the triplet convection scheme of *Hack* [1994] simulates shallow convection. An explicit, non-local atmospheric boundary layer (ABL) parameterization is incorporated into the vertical diffusion parameterization [*Holtslag and Boville*, 1993]. A one dimensional land surface model [*Bonan*, 1996] including a six layer soil column model interacting with the atmosphere enable exchange of energy, momentum, water and carbon dioxide between the atmosphere and land. The absorptivity-emissivity formulation of *Ramanathan and Downey* [1986] is employed to represent the long wave radiative transfer.

[8] Since our primary objective is to study the dynamics of internal IAV, a control simulation for 35 years is conducted with December 1 initial condition and climatological monthly mean sea surface temperature (SST). The climatological mean SST data is derived from *Reynolds and Smith* [1994]. With the solar forcing as well as the boundary forcing (SST) being only annually varying, no external forcing with interannual period forces the model simulations. The simulated interannual atmospheric variability, therefore, arises due to internal feedbacks within the system. We refer to it as internal IAV. The daily mean outputs are examined in this study. This simulation is labeled as CLIM run. Another simulation with the same model was carried out for 20 years forced with observed *Reynolds and Smith* [1994] monthly mean SST and will be labeled as OBSST run. This simulation will be used to examine whether the interannually varying SST influences the climatology of the model simulations and statistics of the simulated ISOs.

[9] We have used low level circulation and precipitation data from observations. The circulation data is derived from National Centers for Environmental Prediction/National Center for Atmospheric Research (NCEP/NCAR) reanalysis [*Kalnay et al.*, 1996; *Kistler et al.*, 2001]. The rainfall data is taken from Climate Prediction Center Merged Analysis of Precipitation (CMAP) [*Xie and Arkin*, 1996]. The pentad CMAP used same algorithm and data sources as the monthly CMAP and is obtained from Climate Prediction Center, Washington D.C., U.S.A. Both circulation data and CMAP are taken for a period of 24 years (1979–2002). The observed data is used to compare the characteristics of the model simulated seasonal mean climate as well as the intraseasonal variability. The amplitudes of the interannual variability in both these parameters are also compared. For this purpose, the interannual anomalies of the seasonal mean for both observations and simulations are derived in the following way.

[10] Let $P_{i,j}(x, y)$; $i = 1, 2, \ldots N$; $j = 1, 2, \ldots M$ be the variable of interest, where $N = 365$ days and $M =$ Number of years used in the analysis ($M = 35$ for CLIM, $M = 20$ for OBSST, and $M = 24$ for observations). The June to September seasonal (JJAS) mean for each year is defined as

$$\overline{P}_j(x,y) = \frac{1}{122}\sum_{i=1Jun}^{30Sep} P_{i,j}(x,y), \qquad j = 1,2,\ldots M \tag{1}$$

The climatological seasonal mean may be calculated as

$$\overline{\overline{P}}(x,y) = \frac{1}{M}\sum_{j=1}^{M}\overline{P}_j(x,y) \tag{2}$$

and the interannual anomalies of the seasonal mean is defined as

$$\overline{P}'_j(x,y) = \overline{P}_j(x,y) - \overline{\overline{P}}(x,y), \qquad j = 1,2,\ldots M \tag{3}$$

[11] The interannual anomalies of the seasonal mean calculated in this manner from the CLIM simulations represent pure ''internal'' variability of the seasonal mean. Those calculated from OBSST and observations, however, represent 'total' IAV containing contributions from both ''internal'' and ''external'' forcing.

[12] The intraseasonal component of precipitation and low level circulation anomalies from the model and observations are calculated in the following manner. Firstly, the daily climatology is derived based on M years of daily data as

$$\{P\}_i(x,y) = \frac{1}{M}\sum_{j=1}^{M} P_{i,j}(x,y) \qquad ; i = 1,2,\ldots N \tag{4}$$

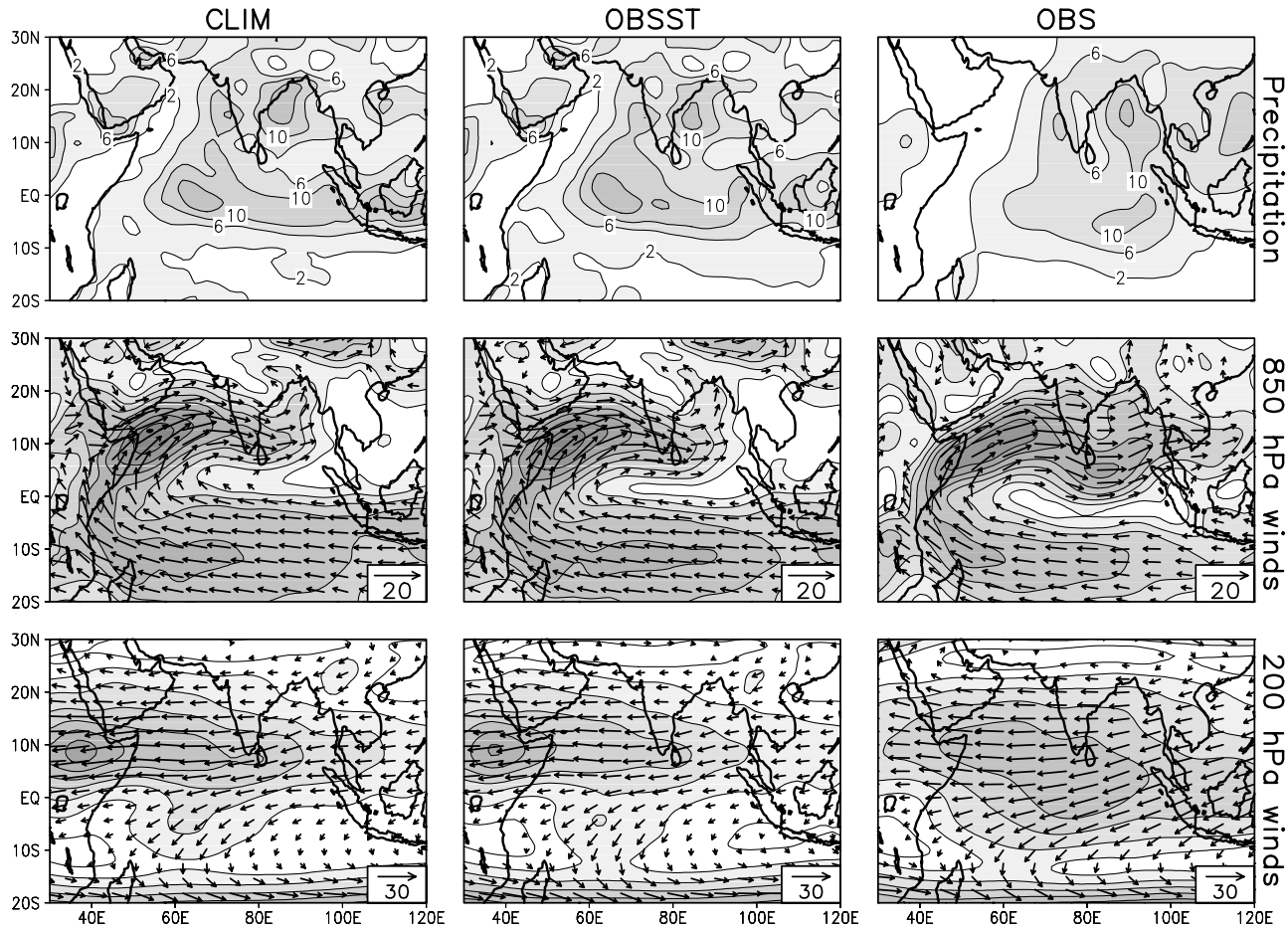

Figure 1. Comparison between simulated and observed June–September (JJAS) climatology. Climatological JJAS precipitation, 850 hPa winds (plotted as vectors and magnitudes are contoured with minimum contour 2 m s^{-1} and contour interval 2) and winds at 200 hPa, plotted as vectors and magnitudes are contoured with minimum contour 4 m s^{-1} and contour interval 4 from the CLIM simulation (left panels), OBSST simulation (middle panels) and observations (Precipitation from CMAP and winds from NCEP, right panels).

[13] This daily climatology is subjected to harmonic analysis and the sum of the annual mean and first three harmonics are extracted. This was done to extract a smoothly varying climatological annual cycle. Let $P^*_i(x, y)$, $i = 1, 2, \ldots N$ be the smoothed climatological annual cycle.

[14] The daily anomalies may be calculated as deviation of the daily values from a climatological mean annual cycle. The daily anomalies are defined as

$$P'_{i,j}(x,y) = P_{i,j}(x,y) - P^*_i(x,y); i = 1,2,\ldots N; j = 1,2,\ldots M \tag{5}$$

[15] Power spectrum analysis was carried out on daily anomalies during the period 1 June to 30 September over certain regions in order to identify the simulated intraseasonal modes. The spectra of both observed and simulated anomalies show two bands of dominant periodicities, one with period between 10 and 20 days and another with period between 30 and 90 days. To investigate the fidelity of the model in simulating the observed spatial structure and propagation characteristics of the two modes, the daily anomalies are filtered using a 10–20 day and a 30–90 day bandpass Lanczos filter (Duchon, 1979).

[16] If the ISOs were a single frequency sinusoidal oscillations, seasonal mean of intraseasonal anomalies would not contribute to the seasonal mean. The fact that the ISOs have a broad band spectrum with periodicities between 10 and 90 days, allows the probability of occurrence of positive and negative phases to be different and could contribute to the seasonal mean. Therefore, to relate intraseasonal anomalies to the seasonal mean, a 10–90 day bandpass Lanczos filter (using 49 weights) is applied to extract the total intraseasonal anomalies. Let us denote the filtered daily anomalies in any of these intraseasonal bands as $\widetilde{P}'_{i,j}(x, y)$. The June to September (JJAS) seasonal mean of intraseasonal anomalies can now be defined as

$$\overline{ISO}_j(x,y) = \frac{1}{122}\sum_{i=1Jun}^{30Sep} \widetilde{P}'_{i,j}(x,y) \quad ; j = 1,2,\ldots M \tag{6}$$

$\overline{ISO}_j(x, y)$ explains the contribution from the intraseasonal timescale to the seasonal timescale and could contribute to the interannual variability. For most of our study, we use the 10–90 day filtered data. Splitting the ISOs into 10–20 day and 30–90 day bands was done only for comparison of

simulated spatial structure and propagation characteristics of the two modes with observed ones. As mentioned in the Introduction, this study examines the relationship between seasonal mean and the intraseasonal variability in terms of the seasonal mean of ISO anomalies as well as the seasonal ISO activity. ISO activity during the summer monsoon season may be defined as the standard deviation of the ISO anomalies during 1 June to 30 September. That is

$$\sigma_{ISO_j}(x,y) = \sqrt{\frac{1}{122}\sum_{i=1Jun}^{30Sep}\left(\widetilde{P'}_{i,j}(x,y) - \overline{ISO_j}(x,y)\right)^2}; j = 1,2,\ldots M \tag{7}$$

3. Model Climatology of Indian Summer Monsoon

[17] While *Meehl and Arblaster* [1998], described some broad aspects of simulated summer climatology of the CCM3, a detailed evaluation of simulation of summer monsoon climatology of the model has not been done. Before proceeding to investigate the cause of the simulated interannual summer monsoon variability, we examine the fidelity of CCM3 in simulating the summer monsoon climatology. June–September climatology of precipitation, 850 hPa winds and 200 hPa winds constructed from the OBSST run as well as from the CLIM run together with similar climatology of observed precipitation from CMAP and winds from NCEP/NCAR reanalysis are also shown in Figure 1. With the simulation of the Bay-of-Bengal (BoB) maximum in precipitation located close to 20°N as in observations, a major systematic error is overcome by CCM3. The western coast of India maximum in precipitation as well as the secondary maximum just south of the equator between 80°E and 100°E are also well represented by the model in both the simulations. The model tends to produce higher precipitation (between 10% and 20%) in all three observed high precipitation regions. The model has significant systematic bias in simulation of climatological mean summer precipitation, over the equatorial region between 55°E and 70°E and 5°N and 5°S where the model simulated precipitation is nearly twice as large as the observed. Another systematic bias of the model simulations is the unrealistic large precipitation over Arabia. On the other hand, the model has a dry bias over the south China Sea and eastern China. The pattern correlation between the simulated and observed precipitation climatology over the region between 40°–110°E and 20°S–25°N is 0.61 (significant at 99% level).

[18] The model simulates location of low level jet, the cross equatorial flow and the south equatorial easterlies well. However, consistent with slightly stronger simulated monsoon precipitation, the simulated maximum wind speed of the low level jet (LLJ) is about 10% stronger than that observed. The pattern correlation between the simulated (OBSST) and observed (NCEP) zonal and meridional wind climatology at 850 hPa are 0.90 and 0.85 respectively. Consistent with the dry bias of the model over the south China Sea region, the simulated 850 hPa zonal winds tend to terminate around 100°E instead of extending to about 120°E as in observations. The strength of the upper level (200 hPa) easterly jet is close to the observed one over the equatorial Indian Ocean. The turning of the easterlies to westerlies (region of minimum wind speed) around 15°S is also well simulated. However, the maximum strength of the model simulated easterly jet tends to occur around 40°E compared to 75°E in observations. The westward shift of the maximum of the easterly jet speed in the model climate may be partly due to unrealistic summer precipitation simulated by the model over Saudi Arabia. The local Hadley circulation with ascending motion in the region (around 20°N) would be associated with equatorward flow at upper level leading to strong easterly flow at these longitudes. The pattern correlation between simulated and observed zonal and meridional winds at 200 hPa are 0.94 and 0.71 respectively.

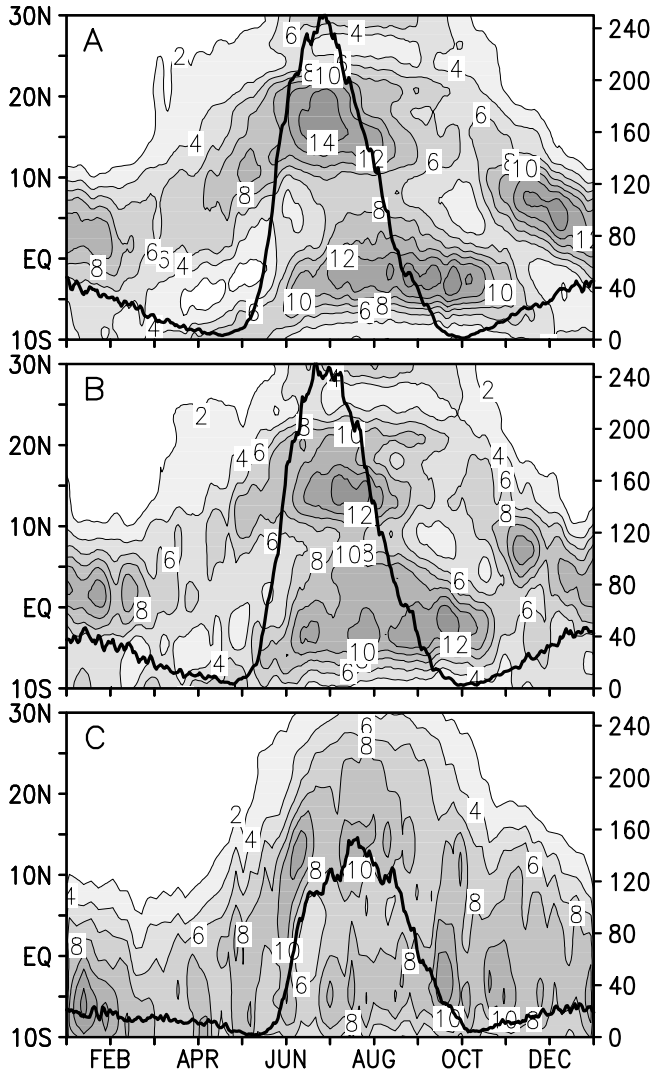

Figure 2. Latitude-time plot of daily climatological mean precipitation (mm day^{-1}) averaged over the longitudinal belt 70°–100°E (a) from CLIM, (b) from OBSST simulations and (c) from observations. Kinetic energy (m^2 s^{-2}) at 850 hPa of daily climatological winds averaged over the region 50°–65°E, 5°–15°N are shown as lines in each panel with scale on the right.

Table 1. Comparison of Simulated and Observed Seasonal Means and Interannual Standard Deviations of EIMR and KELLJ

	Mean			Standard Deviation		
Indices	CLIM	OBSST	OBS	CLIM	OBSST	OBS
EIMR	8.96	8.92	8.20	0.61	1.27	0.76
KELLJ	139.15	144.39	111.18	11.96	17.19	6.90

[19] The onset of the summer monsoon with rather sharp increase of kinetic energy of the low level winds and rapid northward shift and establishment of the tropical convergence zone (TCZ) over the land are important component of annual evolution of the Indian monsoon. The model's ability to simulate the annual evolution of the Indian monsoon is examined in Figure 2. Daily climatological mean precipitation simulated by the model averaged over 70°E–100°E as a function of latitude (shaded contours in Figures 2a and 2b) is contrasted with similar plot for observed precipitation (CMAP, Figure 2c). It is noteworthy that during the summer monsoon season (June–September), the model simulates the two preferred latitudinal locations of precipitation, one over the continent and the other over the equatorial Indian Ocean with a minimum in between quite well except that the simulated precipitation is about 10–20% stronger than observed over both the locations. However, the simulated annual evolution of the precipitation belt has a significant systematic bias during northern winter (November–February) when it remains at around 5°N (Figures 2a and 2b) instead of moving southward to about 5°S as is observed (Figure 2c). As a result, the model simulation of precipitation is characterized by a rather gradual advance of the rain belt from beginning of May establishing the monsoon in June over land (Figures 2a and 2b) and lacks the relatively abrupt northward shift of the rain belt in the beginning of June as seen in observations (Figure 2c). This bias is also seen in the simulated KE of the low level jet over the Arabian Sea as shown as curves in Figure 2. The model monsoon onset takes place about 2 weeks earlier than observed and withdraws about one week prior to observed withdrawal. Consistent with stronger than observed low level winds (Figure 1), the KE of the LLJ is significantly stronger than observed during June and July.

[20] It may be noted that the mean character of the summer monsoon in both the simulations is almost identical. It implies that the simulated mean monsoon is not seriously affected by the interannual SST variations. The simulation of IAV of the seasonal mean by a model could be dependent on the climatology of the model. Since the climatology of CLIM run is almost identical to that of the OBSST run, the internal IAV simulated by the CLIM run is unlikely to be seriously biased on account of the climatology being biased.

4. Simulated Internal IAV of Indian Summer Monsoon

[21] In the absence of any external interannual forcing, any significant IAV of the monsoon simulated by the model in the CLIM run must arise from internal atmospheric dynamics. Part of the simulated IAV could arise from soil moisture feedback as the soil moisture in the model is interactive. Does the model simulate significant IAV of the monsoon? Even if it does, does the spatial structure of the simulated IAV have any similarity with that of the observed IAV of the summer monsoon? These questions are examined in this section. For this purpose, we construct two indices representing the strength of the Indian summer monsoon. First index is the extended Indian monsoon rainfall index (EIMR) represented by June–September mean precipitation averaged over 70°–110°E, 10°–25°N similar to the one suggested by *Goswami et al.* [1999]. This index represents the non-adiabatic heating associated with the Indian summer monsoon better than the traditional index of monsoon as precipitation averaged over the continental India alone [*Goswami et al.*, 1999]. As the low level winds over the Arabian sea are strongly related to the heating over the Indian monsoon region, a second summer monsoon index is constructed as the kinetic energy (KE) of the low level jet (KELLJ) defined as the seasonal mean KE of winds at 850 hPa level averaged over 50°–65°E, 5°–15°N. Long term mean and interannual standard deviation of these indices are shown in Table 1 and compared with corresponding values from the OBSST run and from observations. The observed EIMR is calculated from CMAP data while the observed KELLJ is constructed from NCEP reanalysis. As could be expected from the discussions in the previous section, the long term mean of the indices are close to the observed values. The amplitude of internal interannual variability (CLIM run) of EIMR simulated by CCM3 is about one half of that simulated when forced with observed SST (OBSST run) and is comparable to that observed. This result is broadly similar to the results obtained using GFDL climate model [*Goswami*, 1998] and estimates made using observations [*Ajayamohan and Goswami*, 2003]. Thus, the model does simulate significant internal IAV of the summer monsoon. The IAV of the KELLJ is, however, much larger than that observed (Table 1). The IAV of the indices normalized by their own standard deviation are shown in Figure 3. It is clear that the two indices are strongly correlated with each other (r = 0.86). Therefore, it is a bit puzzling to note that IAV of KELLJ is stronger than observed while

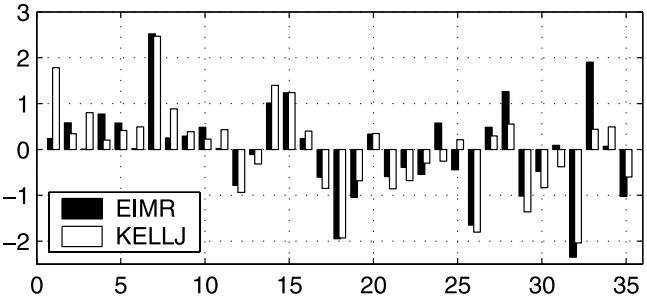

Figure 3. Simulated interannual variations of Indian summer monsoon. EIMR is defined as anomaly of June–September (JJAS) mean precipitation averaged over 70°–110°E, 10°–25°N. KELLJ is defined as anomaly of JJAS mean kinetic energy of winds at 850 hPa level averaged over 50°–65°E, 5°–15°N. Both these indices are normalized by their own standard deviations. Correlation between the two indices is 0.86.

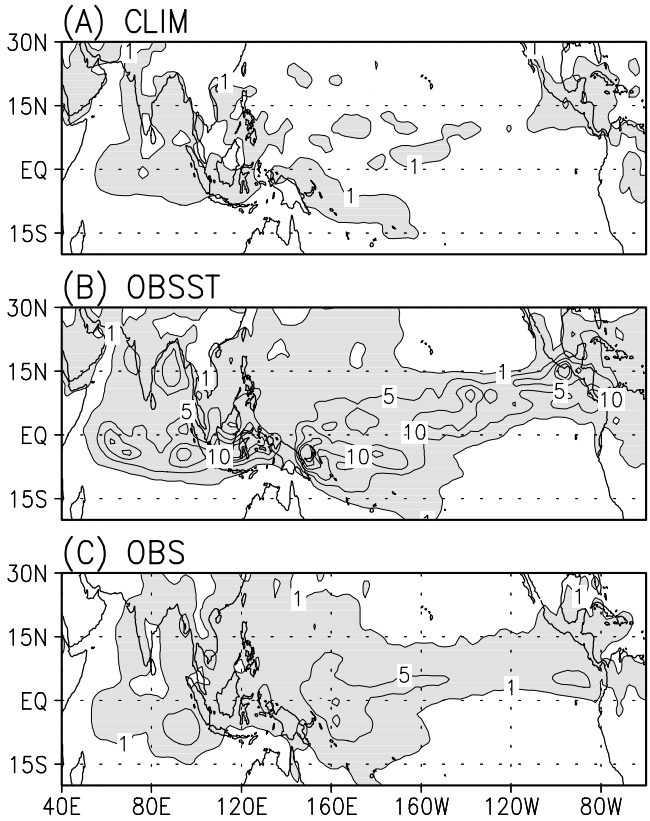

Figure 4. Interannual variance ($mm^2\ day^{-2}$) of seasonal mean precipitation from (a) CLIM, (b) OBSST and (c) CMAP observations.

that of EIMR is weaker than observed. The reason for this discrepancy will be clear when we examine the spatial structure of the IAV. To examine the spatial distribution of amplitude of IAV simulated by the model, the interannual variance of seasonal mean precipitation from CLIM run, OBSST run and from CMAP are shown in Figure 4. It may be noted that in the absence of interannually varying SST, the CLIM run simulates little IAV of seasonal mean precipitation in the central and eastern Pacific. However, significant IAV is simulated over the Asian monsoon region even in the absence of interannually varying SST. One systematic bias is that the model simulates too large IAV over the equatorial IO between 55°E and 70°E compared to observations.

[22] To examine the large scale structure associated with the simulated internal IAV of the summer monsoon, composite of precipitation and 850 hPa winds corresponding to simulated strong and weak monsoons are created. Strong (weak) monsoons are selected from the 35 year simulations depending on whether the normalized EIMR index is greater than 0.75 (less than −0.75) (Figure 5). Composites of strong and weak summer monsoon of simulated precipitation and 850 hPa winds were constructed based on 7 strong years and 6 weak years. The strong minus weak composite of simulated monsoon precipitation and 850 hPa winds are shown in Figure 5a. Strong (weak) observed monsoon is also defined by normalized observed EIMR being greater than 0.75 (less than −0.75). Such strong minus weak summer monsoon composites of precipitation and 850 hPa winds from observations are shown in Figure 5b. To start with, we note that the internally generated IAV of the Indian summer monsoon has large spatial scale similar to the observed summer monsoon interannual variability. The simulated precipitation anomalies have a meridional bimodal structure similar to the one associated with the observed strong (weak) summer monsoon anomalies. The summer monsoon precipitation belt with one center in BoB and another along the western Ghat is well simulated except that the BoB center is stronger in simulations than the western Ghat one while reverse is the case in observations. The south westerlies and the large scale cyclonic vortex associated with the simulated strong (weak) monsoon bear reasonably good correspondence with those associated with observed strong (weak) monsoons. The simulated monsoon trough is shifted eastward compared to the observed location consistent with simulated stronger precipitation center being located eastward of the observed one. The east-west pattern of precipitation anomalies associated with simulated strong (weak) monsoon between the equator and 10°S is, however, quite different from that associated with observed strong (weak) monsoon. This reflects in some discrepancy between the simulated and observed low level winds over this region.

[23] Consistent with the observation made in Table 1 that amplitude of simulated IAV of KELLJ is larger than observed, we note that the strength of the wind anomalies

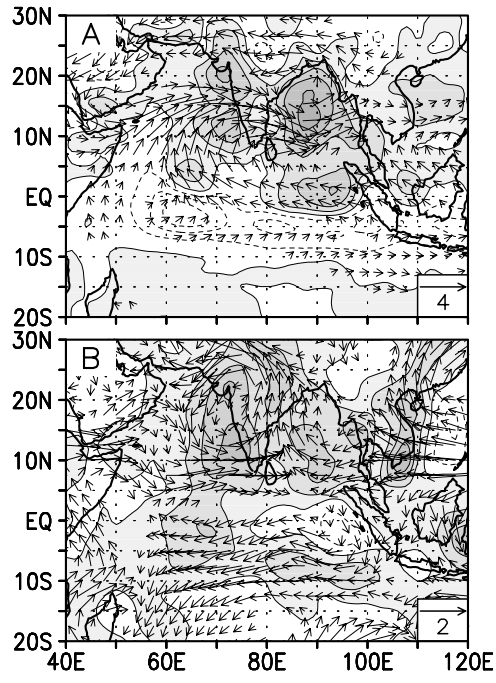

Figure 5. Strong minus weak monsoon composites of anomaly of JJAS mean precipitation (contoured with contour interval 1 mm day^{-1}) and 850 hPa wind vectors ($m\ s^{-1}$) (a) from OBSST simulations based on 7 strong and 6 weak years and (b) from observations (CMAP for precipitation and NCEP reanalysis for winds) based on 6 strong and 5 weak years. Strong (weak) monsoon years are identified based on normalized EIMR greater (less) than 0.75 (−0.75). Scale for wind anomalies is shown in the inset box.

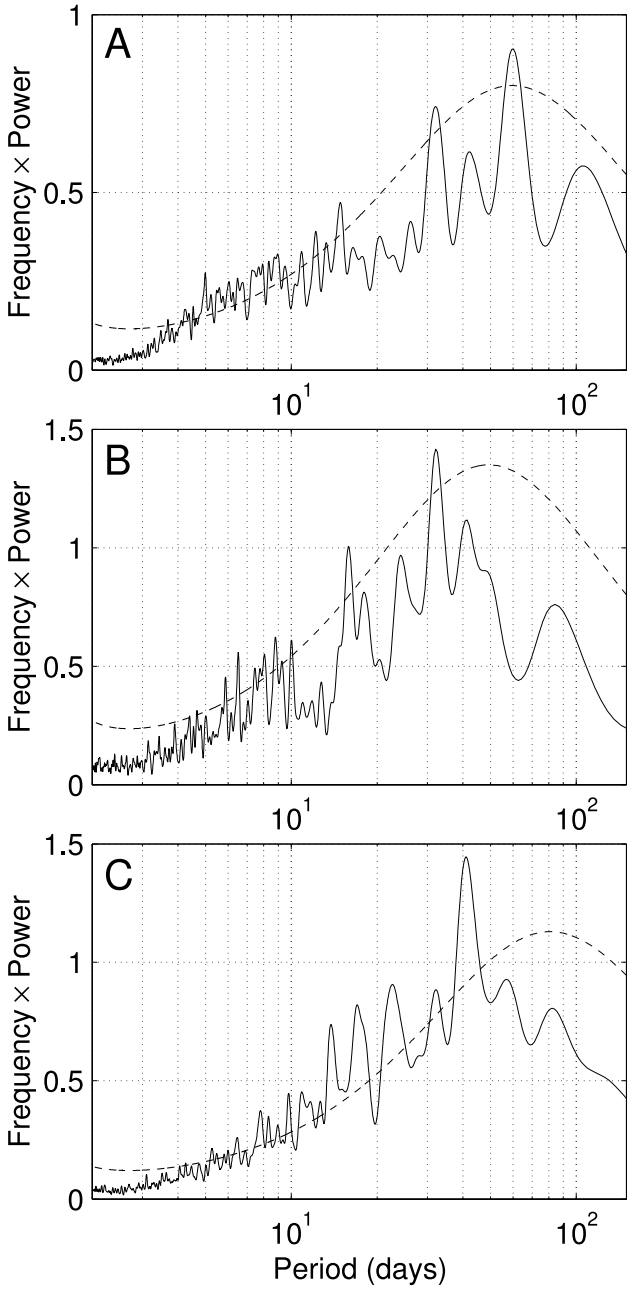

Figure 6. (a) Power spectrum of daily U850 anomalies for the period between 1 June and 30 September averaged over 60°–70°E, 10°–15°N from CLIM simulations. (b) Same as Figure 6a, but for U850 from NCEP reanalysis for the period 1979–2002. (c) Power spectrum of daily precipitation anomalies for the period between 1 June and 30 September averaged over the region 85°–95°E, 10°–20°N from all model simulations. Dashed curves in each panel represent the 95% confidence limit.

over Arabian Sea LLJ area is stronger than that observed over the same area during strong (weak) monsoon (Figure 5). This feature can be related an anomalous feature of simulated rainfall anomalies. Note from Figure 5a that strong (weak) simulated monsoon is associated with a region of negative (positive) precipitation anomaly between 60°E–70°E centered around 5°S while it is positive in observations (Figure 5b). This essentially represents decrease (increase) of large simulated climatological precipitation in this region during strong (weak) monsoon. Linear response of the atmosphere to positive precipitation anomalies to the north (western coast of India and BoB) and negative anomalies to the south during a strong monsoon is consistent with stronger wind anomalies over the LLJ area. During simulated weak monsoon the north-south dipole pattern of precipitation anomalies reverse in sign and is associated with strong wind anomalies of opposite sign. This process leads to stronger IAV simulated wind anomalies in this region.

[24] Thus, even though the GCM simulations have some biases, climatology of GCM simulated summer monsoon is reasonable and it simulates internal IAV of summer monsoon comparable in amplitude to observed amplitude of IAV of the summer monsoon. As the simulated variability in CLIM is entirely that of internal origin, an exact correspondence between the spatial structure of the simulated IAV and observed IAV is not to be expected. Broad similarity between the two provides the basis to use the model simulations to learn more about the dynamics of the internal IAV.

5. Simulated Monsoon Intraseasonal Variability (ISV)

[25] Our working hypothesis is that the ISOs are responsible for the IAV of the seasonal mean. For a meaningful test of this hypothesis, the statistics of the ISOs simulated by the model should be realistic. Therefore, temporal and spatial characteristics of the simulated ISOs during northern summer season (June–September) from both the model simulations (CLIM and OBSST runs) are examined here and compared with corresponding characteristics of observed ISOs. To examine the temporal characteristics, a 850 hPa zonal wind (U850) time series is created with daily anomalies between 1 June and 30 September for all simulated years averaged between 60°–70°E, 10°–15°N. Observed zonal wind time series is obtained from daily anomalies of zonal winds at 850 hPa from NCEP reanalysis. To examine the temporal characteristics of simulated precipitation anomalies, a precipitation time series is created with daily anomalies between June 1 and September 30 for all years averaged between 85°–95°E, 10°–20°N. One reason for selecting these two boxes is that they are regions of large intraseasonal variance of zonal winds at 850 hPa and precipitation respectively. The other rational for selecting them is that the atmospheric response of fluctuations of the heat source over the BoB is expected to generate fluctuations of zonal component of LLJ over the Arabian Sea. The power spectra of the zonal wind time series from CCM3 and from observation are shown in Figures 6a and 6b. The model captures the approximate 15-day and 35-day peaks of the observed spectrum. However, the model simulates a strong 60-day peak not found in observations. The amplitude of zonal wind ISOs is somewhat weaker than that is observed. The power spectrum of precipitation over the BoB (Figure 6c) has reasonable correspondence with that of the simulated zonal winds over the LLJ region (Figure 6a). As we do not have daily precipitation over the same region

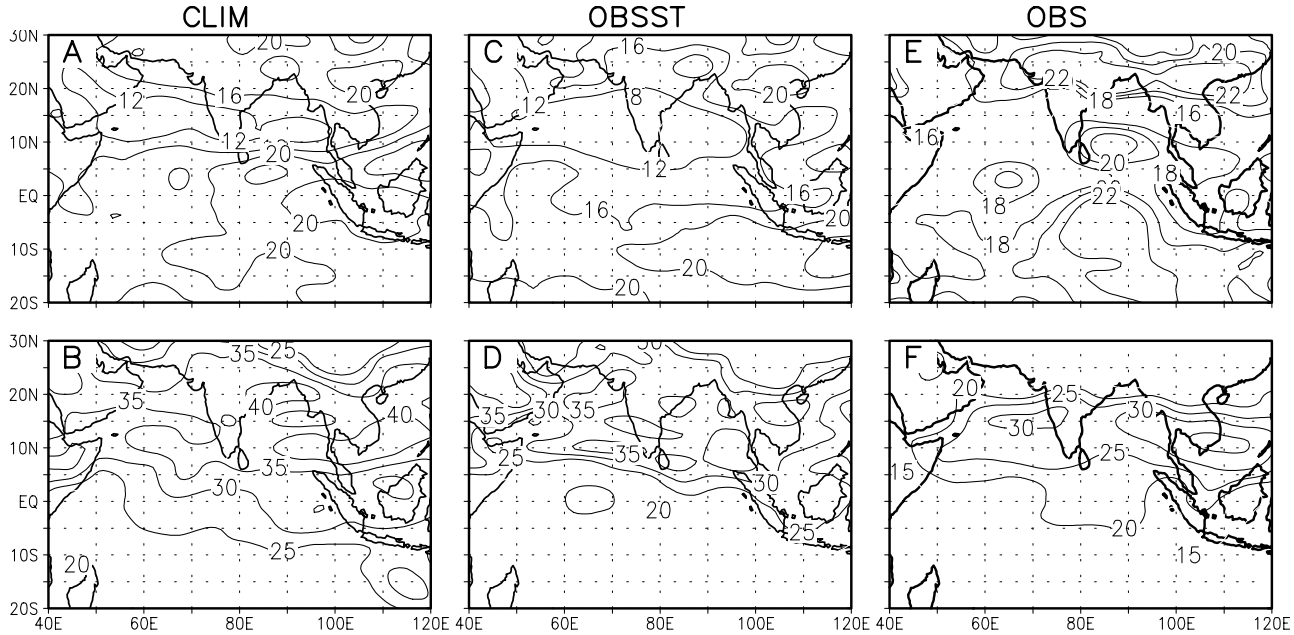

Figure 7. Percentage of daily variance during the summer season explained by the 10–20 day band (a) and 30–90 day band (b) of zonal wind at 850 hPa in the CLIM simulation (left panels). (c) and (d) Same as Figures 7a and 7b, but from OBSST (middle panels). (e) and (f) From NCEP (right panels).

for a reasonable length of time, a comparison of the simulated precipitation spectrum with observation is not possible. All the spectra are calculated using the Tukey window method and the dashed line corresponds to 95% confidence level based on a rednoise null hypothesis.

[26] In order to facilitate comparison of the simulated structure and propagation characteristics of the 10–20 day mode and the 30–90 day mode with corresponding observations, a brief account of the observed characteristics of the two modes are summarized here. Several studies [*Krishnamurti and Bhalme*, 1976; *Chen and Chen*, 1993; *Chatterjee and Goswami*, 2004] have shown that many parameters of the Indian summer monsoon show a quasi-biweekly or a 10–20 day oscillation. Such an oscillation is also seen in the western Pacific and maritime continent during the northern winter [*Numaguti*, 1995; *Kiladis and Wheeler*, 1995]. This mode is characterized by a double vortex structure in the low level winds [*Chen and Chen*, 1993; *Chatterjee and Goswami*, 2004] with characteristic zonal scale of about 6000 km and westward phase speed of about 4–5 m s^{-1}. It has been identified with a convectively driven gravest meridional mode Rossby wave modified by the background mean flow [*Chatterjee and Goswami*, 2004]. The lower frequency 30–60 day or 30–90 day mode has a much larger zonal scale associated with it [*Webster et al.*, 1998; *Krishnamurti*, 1985; *Nakazawa*, 1986; *Goswami and Ajayamohan*, 2001] compared to that of 10–20 day mode. First noted by *Yasunari* [1979] and *Sikka and Gadgil* [1980], this mode has a characteristic northward and eastward propagation over the Indian monsoon region. The mode is also associated with repeated northward migration of the tropical convergence zone (TCZ) from equatorial Indian Ocean to the monsoon trough over the Indian continent [*Sikka and Gadgil*, 1980; *Krishnamurti and Subrahmanyam*, 1982]. Both the modes contribute to the active-break cycles of monsoon subseasonal variations.

[27] To study the spatial structure and propagation characteristics of the two modes in some detail, wind anomalies are band-pass filtered using a Lanczos filter to retain periodicities between 10 and 20 days and between 30 and 90 days respectively. Percentage of total daily variance accounted by the 10–20 day mode and the 30–90 day mode of zonal wind during the summer monsoon season are shown in Figure 7. It is noted that the 10–20 day mode explains 15–20% of total daily variance. The 30–90 day mode on the other hand, explains 30–35% of daily variance. Partitoning of total daily variance into 10–20 day mode and 30–90 day mode in simulated zonal winds at 850 hPa bears close resemblence with that in observations.

[28] Mean spatial structure and propagation characteristics of a ISO mode could be studied using lag-regression of ISO anomalies everywhere over the domain of interest with respect to a reference time series [e.g., *Hendon and Salby*, 1999]. In principle, the reference time series could be anywhere in the domain of interest. To study the spatial structure of the 10–20 day mode, a reference time series is created by averaging 10–20 day filtered zonal winds over a box between 85°–90°E and 5°–10°N during the summer monsoon season (1 June to 30 September) for all years of the two model simulations. A similar reference time series of 10–20 day filtered zonal wind at 850 hPa for 24 years (1979–2002) of NCEP reanalysis is also constructed. Regressions of 10–20 day filtered zonal and meridional winds are constructed with respect to the reference time series for both model simulations (CLIM and OBSST runs) as well as for observation (NCEP) with lag-lead of the filtered anomalies with respect to the reference time series ranging from lag of 15 days to lead of 15 days. Simulta-

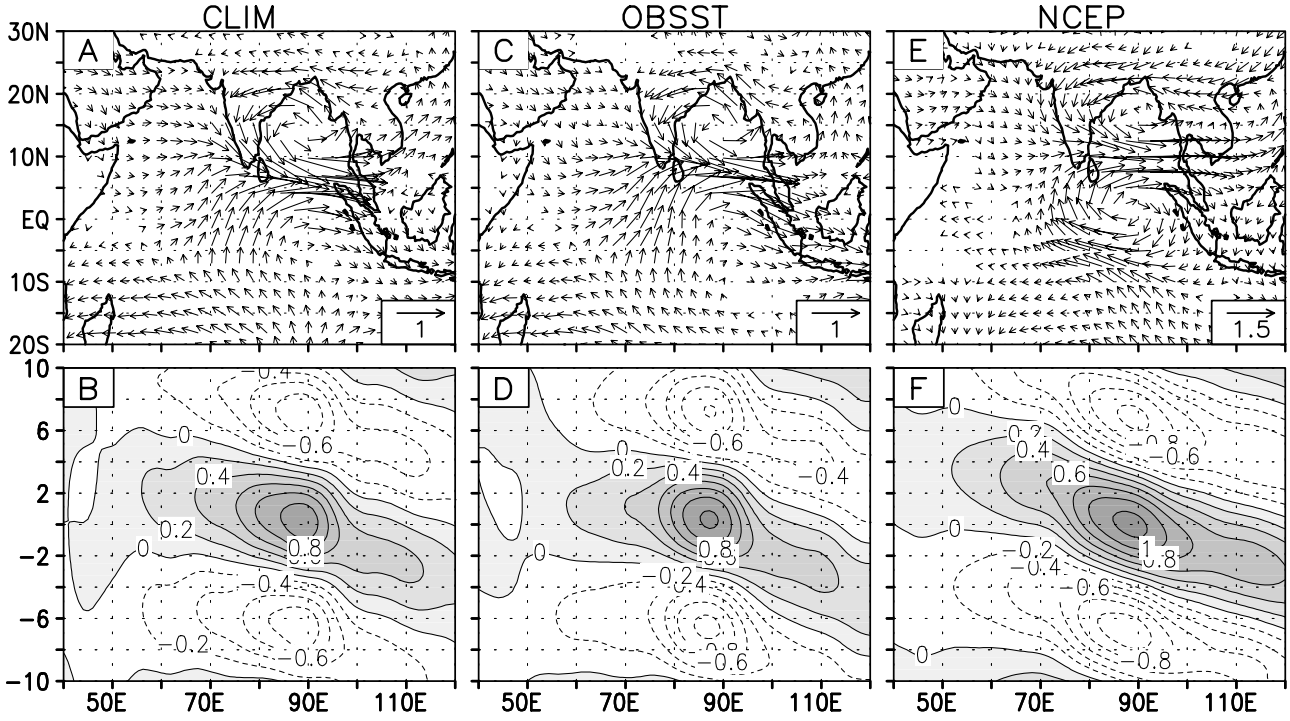

Figure 8. Lag-zero regression of 10–20 day band-passed 850 hPa wind anomalies (m s^{-1}) at all grid points with a reference time series defined as filtered U850 anomalies averaged over 85°–90°E, 5°–10°N and Longitude versus lags (days) plot of regressed U850 anomalies averaged over 5°–15°N from CLIM (left panels), from OBSST (middle panels) and from NCEP reanalysis (right panels).

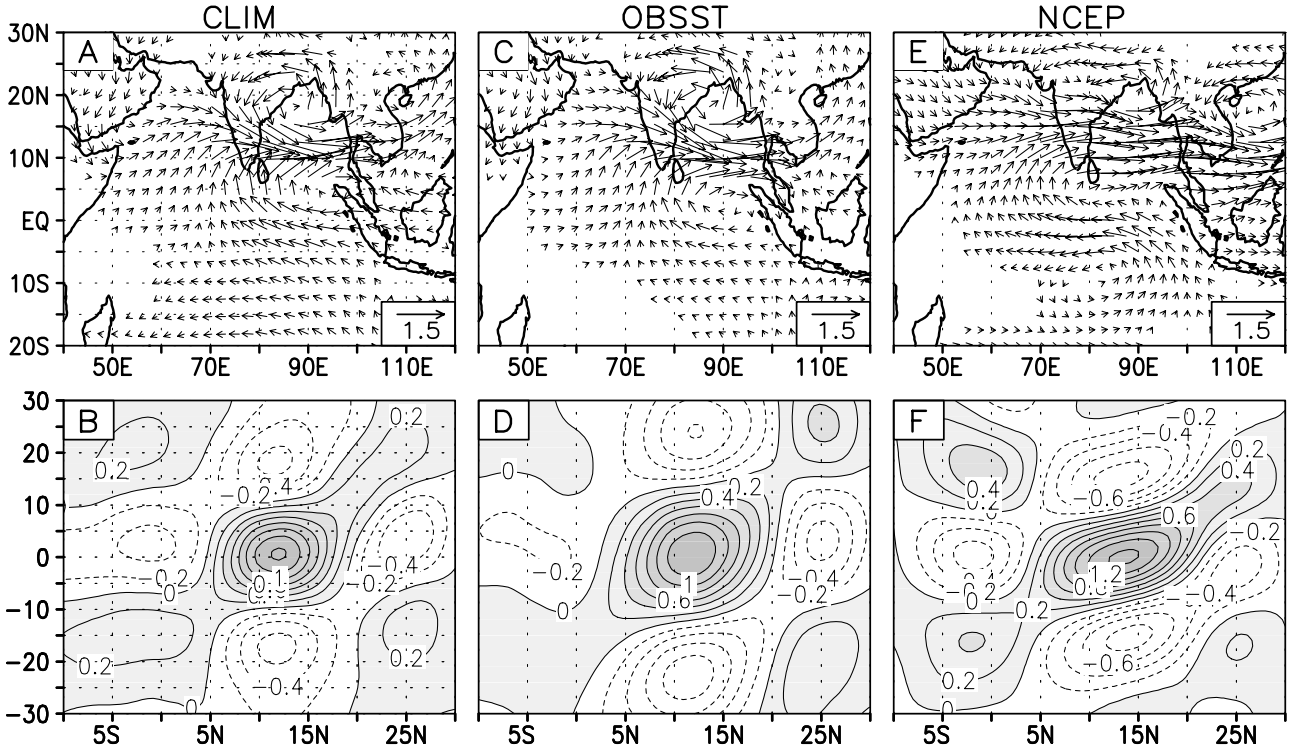

Figure 9. Lag-zero regression of 30–90 day band-passed 850 hPa winds (m s^{-1}) at all grid points with a reference time series defined as filtered U850 anomalies averaged over 85°–90°E, 5°–10°N and Latitude versus lags (days) plot of regressed U850 averaged over 70°–90°E from CLIM (left panels), from OBSST (middle panels) and from NCEP reanalysis (right panels).

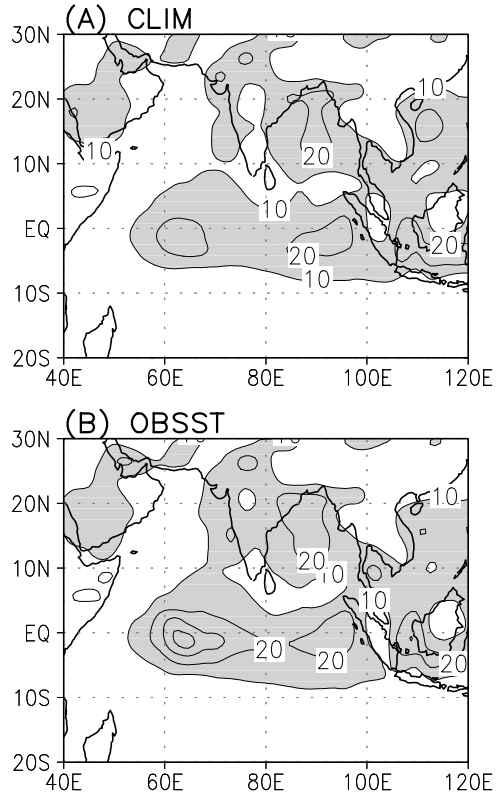

Figure 10. Variance (mm^2 day^{-2}) of 10–90 day filtered intraseasonal anomalies from CLIM (a) and from OBSST (b).

neous regressed vector wind pattern from the two model simulations and NCEP are shown in Figures 8a, 8c, and 8e, respectively. The spatial pattern of the simulated 10–20 day mode having a double vortex structure with one vortex centered around the equator (Figures 8a and 8c) is quite similar to that observed (Figure 8e). It is noteworthy that the amplitude and spatial pattern of the 10–20 day mode simulated in the CLIM run is almost identical to that in the OBSST run. The east-west propagation characteristics of the mode could be seen from the regressed zonal winds averaged over 5°–15°N and plotted as a function of longitudes for all lags and leads (Figures 8b, 8d, and 8f). It may be noted that the westward phase speed of the simulated mode (Figures 8b and 8d) is quite similar to the westward propagation speed of the observed mode (Figure 8d). However, the amplitude of simulated mode is some what weaker than that observed consistent with observations made while comparing of spectra of simulated zonal winds (Figure 6) with that of observed. The spatial structure of the mode in model simulation as well as in observations resemble the gravest meridional mode equatorial Rossby wave shifted to north by about 5° [*Chatterjee and Goswami*, 2004].

[29] The horizontal structure of the 30–90 day mode is studied in a similar manner by constructing a reference time series of 30–90 day filtered zonal winds averaged over 85°–90°E and 5°–10°N and calculating lag regressions of 30–90 day filtered zonal and meridional winds everywhere. The simultaneous vector wind pattern for the mode from the two model simulations as well as from observation are shown in Figures 9a, 9c, and 9e, respectively. The zonal scale of the observed 30–90 day mode (Figure 9e) is much larger than that of the 10–20 day mode (Figure 8e). Both the model runs simulate the observed horizontal structure of the mode reasonably well (see Figures 9a and 9c). The pattern correlation between model simulated and observed regressions at zero lag for zonal and meridional winds are 0.78 and 0.72 respectively. The 30–90 day mode is known to have northward propagation over the Indian monsoon region. Lag-latitude plot of regressed zonal winds averaged over 60°–90°E are shown in Figures 9b, 9d, and 9f from the two model simulations and NCEP respectively. The simulated 30–90 day mode has northward propagation in the

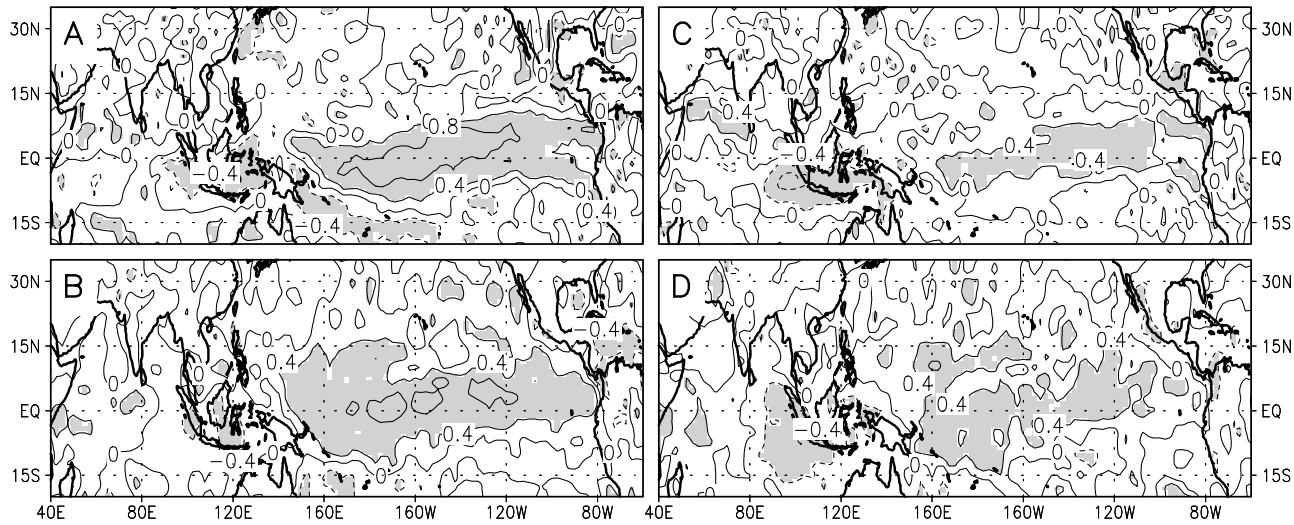

Figure 11. Correlation between JJAS mean Nino3 time series and JJAS standard deviation of ISO anomalies in OBSST (a) and from CMAP (b). The correlation between JJAS mean DMI time series and JJAS standard deviation of ISO anomalies in OBSST (c) and from CMAP (d). Values significant at 95% level are shaded.

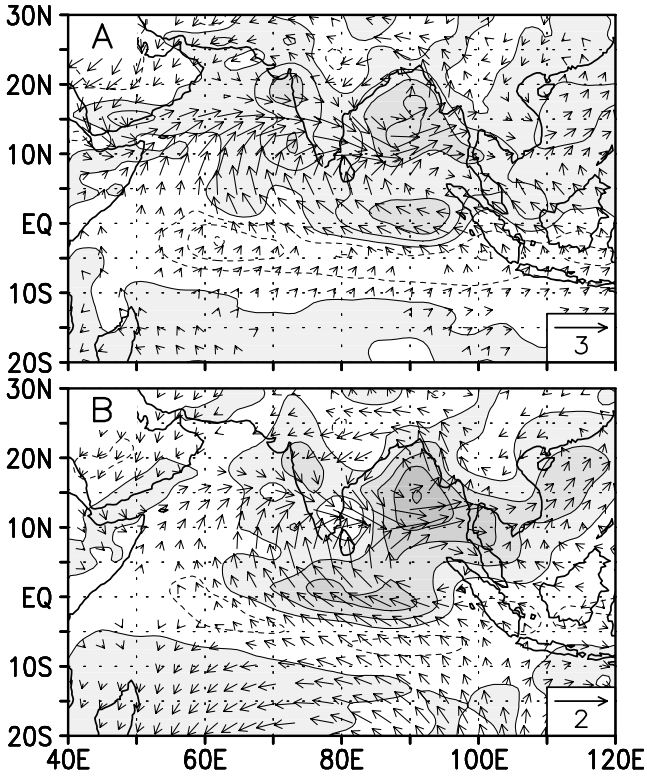

Figure 12. A common spatial mode of intraseasonal and interannual variability of simulated precipitation and low level winds. (a) The CEOF1 of interannual anomalies of simulated seasonal mean of precipitation (contoured with interval 1 mm day^{-1} and positive values shaded) and simulated 850 hPa winds (vectors). (b) The CEOF1 of 10–90 day filtered simulated intraseasonal anomalies of precipitation (contoured with interval 0.25 mm day^{-1} and positive values shaded) and 850 hPa winds (vectors).

Indian monsoon region similar to that observed. However, phase speed for the simulated northward propagation is slightly slower (Figures 9b and 9d) than that observed (Figure 9f). Spatial patterns of intraseasonal variance in CLIM and OBSST simulations are also closely similar (Figure 10).

[30] The fact that the mean statistical properties of the summer ISOs (e.g., large scale variance pattern, partitioning of variance to 10–20 day mode and 30–90 day mode, mean spatial structure and mean propagation characteristics, etc.) are almost identical in the CLIM and OBSST simulations, reinforces the fact that the summer ISOs arise due to internal dynamics (convective instability) of the atmosphere and the interannually varying SST does not significantly alter their statistical properties. This point is further illustrated in Figure 11 where simultaneous correlation between JJAS Nino3 SST with interannual (IA) variation of standard deviation of ISO anomalies during JJAS from the OBSST run is shown (Figure 11a). Similar correlation between IA variations of standard deviation of ISO anomalies during JJAS of observed precipitation (CMAP) is shown in Figure 11b. While the IA variation of ISO activity is strongly correlated with IA variation of SST over the central and eastern Pacific, associated with ENSO, there is little correlation between the two over the Asian monsoon region in observations (Figure 11b) as well as in OBSST simulation (Figure 11a). These correlations indicate influence of interannual SST variations associated with ENSO on IA variations of ISO amplitude. In order to examine whether IA SST variability unrelated to ENSO could modulate ISO variability over the Asian monsoon region, we also show the correlation between IA variation of standard deviation of JJAS ISO anomalies and JJAS mean Indian Ocean Dipole Mode Index (DMI) [*Saji et al.*, 1999]. DMI is defined as the difference of SST between a western box (50°–70°E, 10°S–10°N) and an eastern box (90°–110°E, 10°S–Eq). It is noted that the ISO activity over the Asian monsoon region is not significantly modulated by the Dipole mode related SST variability over the Indian Ocean either. Our hypothesis is that the summer ISOs are responsible for the internal IAV over the Asian monsoon region. Since the ISO activity over this region is not modulated by the IA SST variability (Figure 11), the internal variability is essentially decoupled from the external variability over this region. Therefore, in the next section, we examine how ISOs could influence the seasonal mean monsoon and result in the internal IAV in the CLIM simulation. For the reasons discussed above, we believe that the same mechanism may be applicable for explaining the origin of internal IAV of the Asian summer monsoon in the observations.

6. Mechanism for Internal IAV of Simulated Indian Summer Monsoon

[31] Mechanisms through which the ISOs could influence the seasonal mean and its IAV were outlined in the Introduction. In this section, we provide evidence from the CLIM simulations to support the hypothesis that the internal component of IAV is essentially caused by the ISOs.

[32] Statistical average of ISO anomalies over the season could influence the seasonal mean and its IAV if the spatial structure of the ISOs had significant projection on the spatial structure of the seasonal mean. If this were a major cause of the simulated IAV of the seasonal mean, the spatial structure of IAV of the seasonal mean should also be similar to that of the ISOs. Therefore, the spatial structure of the dominant mode of IAV is compared with that of the ISV. For this purpose, a combined empirical orthogonal function (CEOF) analysis of interannual anomalies of the seasonal mean precipitation and zonal and meridional winds at 850 hPa were carried out. The first EOF of IAV for precipitation and vector winds at 850 hPa are shown in Figure 12a. Similarly, the dominant mode intraseasonal variability of precipitation and zonal and meridional winds at 850 hPa are found by carrying out a combined EOF analysis of 10–90 day filtered anomalies during the summer season (1 June–30 September) for all years taken together. The first EOF of ISV of precipitation and vector winds at 850 hPa are shown in Figure 12b. It is clear that a common spatial mode governs both intraseasonal and interannual variability of precipitation as well as low level winds. The pattern correlation between the ISV and IAV for precipitation and U850 calculated between 50°–110°E, 15°S–25°N are 0.81 and 0.83 respectively. The common spatial mode for ISV and IAV of the seasonal mean provides one evidence

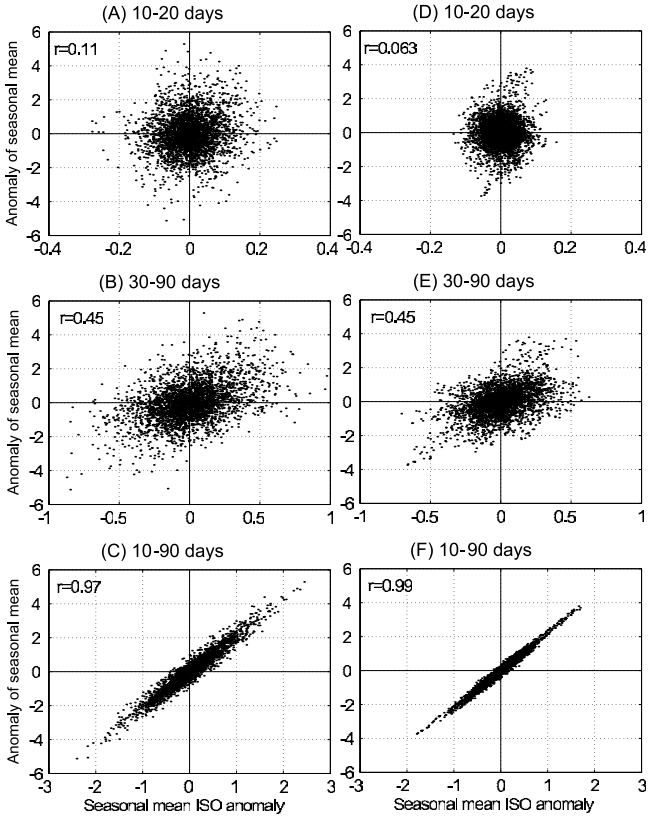

Figure 13. Scatter plot of interannual anomalies of seasonal mean versus seasonal mean of intraseasonal anomalies of precipitation (mm day^{-1}) from (a) 10–20 days band, (b) from 30–90 days band and (c) from 10–90 days band at all grid points in the domain 70°–100°E, 10°–30°N. (d, e, f) Similar to Figures 13a, 13b, and 13c, but for U850. Correlation values are given in the respective panels.

that the ISOs are likely to be responsible for the IAV of the seasonal mean.

[33] We now examine the relationship between the statistical average of ISO anomalies over the season and the anomalies of seasonal mean. The anomaly of seasonal mean and seasonal mean of ISO anomalies of precipitation and U850 at each grid point over the Indian monsoon region (70°E–100°E, 10°–30°N) are plotted as scatter diagram in Figures 13c and 13f, respectively. The strong correlations suggest that the relationship between the seasonal mean of ISO anomalies and that of the anomaly of the seasonal mean is valid at all grid points. Hence, the similarity between the spatial structure of the ISO mode and IAV of the seasonal mean may be helpful but not essential for this mechanism to work. It is, therefore, essential to understand how these seasonal ISO bias is generated.

[34] Could statistical average of ISO anomalies within the individual bands of 10–20 days and 30–90 days influence the seasonal mean? To investigate this issue, anomalies of seasonal mean and seasonal mean of ISO anomalies of precipitation and U850 at each grid point over the same region in the 10–20 day and 30–90 day bands are plotted as scatter diagram in Figures 13a, 13b, 13d, and 13e. Several points are noteworthy in this figure. Firstly, seasonal mean of ISO anomalies within the individual bands do not correlate well with the anomaly of the seasonal mean while that of full ISO anomalies correlate strongly with the seasonal mean. Also, it may be noted that the seasonal mean 10–90 day filtered anomaly is much larger than the linear sum of seasonal mean of 10–20 day and 30–90 day filtered anomalies. ISO anomalies in individual bands (10–20 days and 30–90 days) are rather periodic and hence contribute little to the seasonal mean. However, taken together, the total ISO signal (10–90 days) represents a broad-band spectrum and hence aperiodic. This aperiodicity is responsible for the significant seasonal mean anomaly. The aperiodicity or the broad band character of the ISO is caused by the non-linear interactions between the bands and with high frequency synoptic disturbances.

[35] The non-zero seasonal mean of ISO anomalies is essentially a result of the non-Gaussian nature of the PDF of the ISO anomalies. In other words, stronger (weaker) seasonal mean is a result of higher frequency of occurrence of the positive (negative) phase of the ISOs. This may be illustrated by the difference in frequency of occurrence of intraseasonal precipitation anomalies during strong and weak monsoon years in the model simulations. Seven strong monsoon years and six weak monsoon years were identified from the model simulations using +0.75 (−0.75) normalized EIMR to delineate strong (weak) monsoons. The frequency distribution of intraseasonal precipitation anomalies averaged over 70°–100°E, 10°–30°N are shown in Figure 14. It is clear that strong (weak) monsoon in the model is characterized by higher frequency of occurrence of positive (negative) intraseasonal anomalies. Thus, a major mechanism for producing IAV of the model climate is essentially residual influence of the ISV. The fact that seasonal mean of ISO anomalies of zonal wind also correlate strongly with the anomaly of the seasonal mean similar to that for the rainfall indicates that it represents a fundamental mechanism of producing internal IAV.

[36] We have established how the broad-band nature of the ISO spectrum is instrumental in generating biases in the seasonal mean of ISO anomalies for both precipitation and zonal winds. For the precipitation, apart from the broad-band character, that results in residue of the seasonal mean ISO anomalies, there is also a statistical relation that generates the seasonal mean of ISO anomalies, which eventually can contribute the seasonal mean precipitation. The probability density function of precipitation is closer to a binomial distribution. For such a distribution, variance is proportional to the mean. Therefore, a region with a larger probability of rainfall will have larger variability in all the frequency bands and will tend to have a higher mean. This argument is exactly valid for unfiltered precipitation anomaly time series. For ISO anomalies (10–90 day filtered) the approximate binomial behavior is still applicable albeit slightly diluted.

[37] Some evidence supporting the non-linear mechanism comes from the the fact that the regions of high ISV are also regions of high IAV of seasonal ISO bias and regions of high IAV of the seasonal mean. The variance of the 10–90 day filtered ISO anomalies of precipitation during the summer season is calculated for each year and an average ISO variance for the 35 years is constructed. This is

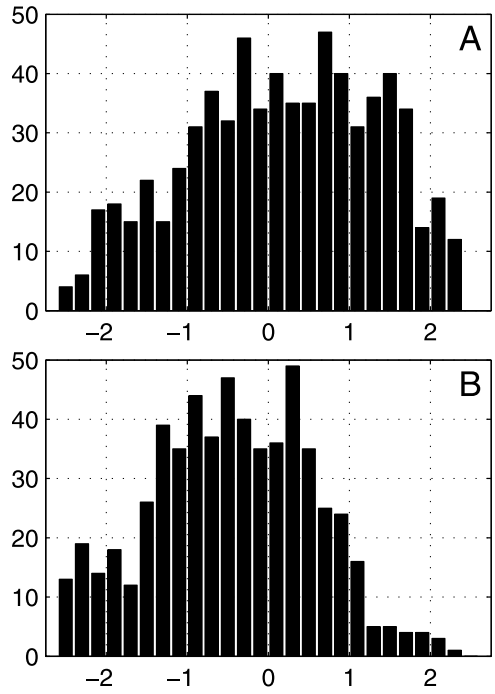

Figure 14. Histogram of normalized intraseasonal anomalies (10–90 day filtered) of precipitation averaged over 70°–100°E, 10°–30°N for (a) 7 strong monsoon years and (b) 6 weak monsoon years. Strong (weak) monsoon years are identified based on normalized EIMR greater (less) than 0.75 (−0.75).

shown in Figure 15 where the spatial distributions of ISO variances (Figure 10a) are compared with their counterpart of interannual variances of seasonal ISO bias (Figure 15a) and interannual variations of the seasonal mean (Figure 15b). Striking similarity between the mean intraseasonal variance and interannual variance of seasonal ISO bias arises from the non-linear process (Figures 10a and 15b). Also the linear relation between IAV of seasonal ISO bias and IAV of seasonal mean is evident (Figures 15a and 15b). The relationship between the ISO amplitude and IAV of seasonal mean further illustrated in Figure 16 where the seasonal mean precipitation and amplitude of ISO activity (standard deviation) at each grid point over three regions (Indian monsoon region, equatorial Indian Ocean and equatorial western Pacific) are shown. The average value of seasonal mean for each bin of ISO amplitude is plotted and the scatter is shown in the form of error bars. Although linear correlation is shown in each panel, the relationship is linear only when the ISO activity is weak, consistent with the binomial principle. For higher amplitude of ISO activity, the relationship is non-linear with higher scatter of seasonal mean for the same value of ISO activity. Figure 16 has a lot of similarity with similar plot between sea surface temperature and convective activity [*Gadgil et al.*, 1984]. The phase space dimension of the simulated ISOs being quite high, it not possible to isolate the exact non-linear mechanism through which the ISOs influence the seasonal mean.

[38] Lastly, we also note that seasonal mean of ISO anomaly (Figure 13c) explains only about one half of the simulated interannual anomaly of the seasonal mean. This indicates that the the ISOs do control the nature of the IAV but the linear effect of projection of the ISO mode onto the interannual mode is significantly amplified by some non-linear interactions within the system. These could be the interaction between ISOs and the synoptic variability, land surface processes, etc.

7. Conclusions and Discussions

[39] Seasonal mean prediction and predictability experiments with GCMs indicate that a significant fraction of observed interannual variability (approximately 50% or more) of the Indian summer monsoon may be due to internal low frequency variability. The internal LF variability act as a background of unpredictable noise mixed with the predictable externally forced signal. Improvement in seasonal mean prediction would require successful extraction of the signal from the background noise of comparable magnitude. In order to develop such a technique, a clear understanding of physical mechanism(s) responsible for the internal IAV is required but is not currently available. The objective of the present study has been to attempt to unravel the mechanism responsible for the observed internal IAV of the ISM. However, a clean separation between the internal and external component of IAV is not feasible from observations, from CGCM simulations or from simulations of AGCM with obserserved SST as boundary forcing. Hence, it is not possible to gain insight on the dynamics of the observed internal IAV from observations or from such model experiments. However, some insight regarding the basic dynamics of internal IAV could be gained if the

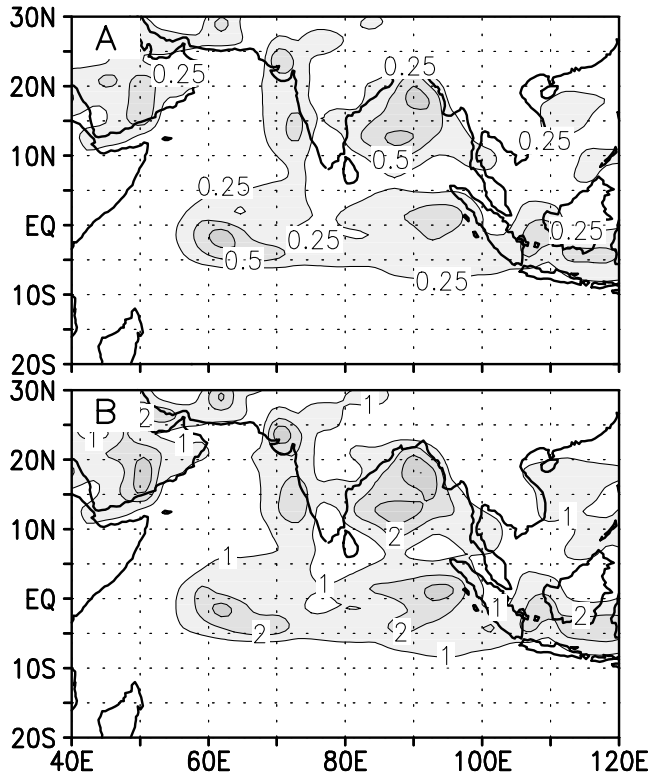

Figure 15. Interannual variance of seasonal ISO bias (a) and the interannual variance of seasonal mean (b) of precipitation.

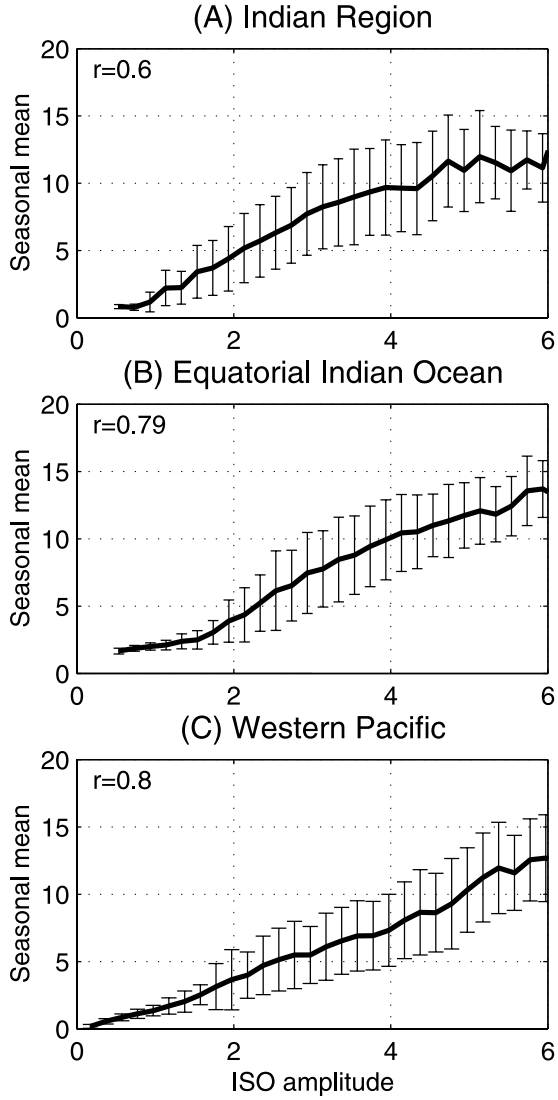

Figure 16. Relationship between seasonal mean and amplitude (standard deviation) of 10–90 day filtered intraseasonal anomalies of precipitation (mm day^{-1}). (a) The Indian monsoon region (70°–100°E, 10°–30°N), (b) equatorial Indian Ocean (70°–100°E, 10°S–10°N) and (c) equatorial western Pacific (120°–160°E, 10°S–10°N). The thick line shows the average seasonal mean value in every 0.2 mm day^{-1} bin of ISO amplitude and the error bars represent the standard deviation of seasonal mean in each bin. Linear correlation values are given in the respective panels.

internal component could be decoupled from the external component. We attempt to achieve this by trying to understand the mechanism responsible for internal IAV generated in a GCM experiment. This is done by integrating an AGCM (CCM3 with T42 horizontal resolution and 18 levels in the vertical) for a long time without any external interannual forcing. Any interannual variability of the simulated ISM (or any other climate system for that matter) in such an experiment, therefore, is of internal atmospheric origin. It is shown that model simulates interannual variability of the Indian monsoon comparable in amplitude and with spatial structure having broad similarity with the observed interannual variability of the Indian monsoon. As the model simulates significant and reasonable internal IAV of the summer monsoon, an understanding of the model internal IAV may provide insight towards understanding the observed internal IAV. Further, we provide some indication that the internal and external IAV over the Asian monsoon region may not be strongly coupled. Therefore, insight gained from our excercise may be relavant even in explaining the origin of observed IAV of the ISM.

[40] Motivated by some of our earlier work, we start with the working hypothesis that monsoon ISOs are responsible for generating the internal monsoon IAV. For meaningful test of this hypothesis, first, the nature of the simulated ISOs is studied in detail and compared with observed character of the ISOs. It is shown that the model simulates the spatial and temporal structures and the propagation characteristics of the summer ISOs over the Indian monsoon region with reasonable degree of fidelity. However, the amplitude of the simulated ISOs is weaker than that observed.

[41] The spatial structure of the ISOs has significant projection on the seasonal mean such that it strengthens (weakens) the seasonal mean in its active (weak) phase. It is also shown that dominant mode of ISV and that of IAV of the seasonal mean are governed by a common mode of spatial variability. It is further shown that the seasonal mean of total ISO anomalies (not that of 10–20 day filtered or 30–90 day filtered but of the 10–90 day filtered data) correlates strongly with the anomaly of seasonal mean at every grid point. Thus, it appears that the non-trivial seasonal mean (seasonal bias) of ISO anomalies is the primary cause of the internal IAV of the Indian monsoon. While the projection of the spatial structure of the ISOs on the seasonal mean structure is helpful, it is not essential. The non-trivial seasonal mean (seasonal bias) of ISO anomalies, in turn, arise from the aperiodic nature of ISO anomaly time series or non-Gaussian character of their PDF. This is supported by the finding that years of strong (weak) simulated seasonal mean monsoon is associated with higher probability of occurrence of active (weak) ISO conditions. This mechanism of generation of internal IAV may be considered a quasi-linear mechanism as the broadband nature of the ISO anomalies (aperiodic) crucial for the mechanism to work arises from non-linear interaction between the 10–20 day mode and 30–90 day mode and between these modes and other high frequency oscillations.

[42] For precipitation, apart from the broad-band character, that results in residue of the seasonal mean ISO anomalies, there is also a statistical relation that generates the seasonal mean of ISO anomalies, which eventually can contribute the seasonal mean precipitation. The probability density function of precipitation is non-Gaussian and closer to a binomial distribution. For such a distribution, variance is proportional to the mean. Therefore, a region with a larger probability of rainfall will have larger variability in all the frequency bands and will tend to have a higher mean. This is a non-linear mechanism that introduces internal IAV of precipitation. It is found that the regions of high ISV of precipitation are also regions of high IAV of seasonal ISO bias and regions of high IAV of the seasonal mean. In fact, IAV of seasonal mean and that of ISO activity is strongly correlated at all grid points. This relationship is in general

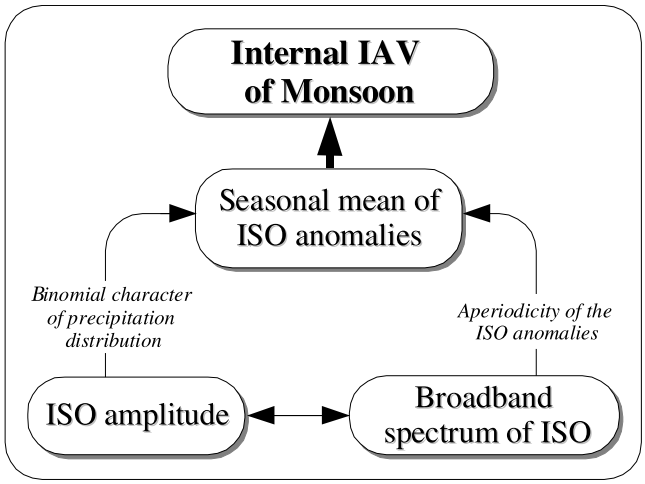

Figure 17. A schematic showing the relationship between ISO and IAV of precipitation through different mechanisms.

non-linear with approximate linear relationship being valid when ISO amplitude is weak. The two mechanisms may not be completely independent from each other. The non-linearity that contributes to the seasonal mean bias through the binomial character also may give rise to the broad-band nature of the ISO spectrum. How the mechanisms contribute to the seasonal mean bias of ISO anomalies and hence to internal IAV of ISM is schematically illustrated in Figure 17.

[43] However, even within the context of the GCM, only about 50% of interannual anomaly of the seasonal mean monsoon is accounted for by the seasonal mean bias of the ISO anomalies. Therefore, there exist other mechanism(s) that also contribute to internal IAV. One such possibility is interaction with soil moisture and ground hydrology. It may be noted that the soil moisture in the model simulations have been determined interactively by the land surface model. In principle, soil moisture feedback could contribute to some simulated internal IAV. Part of the unexplained internal IAV simulated by the model arise from such interactions.

[44] **Acknowledgments.** We are grateful to Department Ocean Development, Government of India, New Delhi, and Indian National Centre for Ocean Information Services (INCOIS), Hyderabad, for a grant and partial support for this work. UCAR/NCAR/CGD is gratefully acknowledged for making the NCAR-CCM3 available. NCEP Reanalysis data are provided by the NOAA-CIRES Climate Diagnostics Center, Boulder, Colorado, USA, from their Web site at http://www.cdc.noaa.gov/. CMAP data are obtained from ftp://ftp.ncep.noaa.gov/pub/precip/cmap. Three anonymous reviewers are gratefully acknowledged for their comments on the earlier version of the manuscript. Thanks are due to R. Vinay for help with the model.

References

Ajayamohan, R. S., and B. N. Goswami (2003), Potential predictability of the Asian summer monsoon on monthly and seasonal time scales, *Meteorol. Atmos. Phys.*, doi:10.1007/s00,703-002-0576-4.

Anderson, J., L. H. van den Dool, A. Barnston, W. Chen, W. Stern, and J. Ploshay (1999), Present day capabilities of numerical and statistical models for atmospheric extratropical seasonal simulation and prediction, *Bull. Am. Meteorol. Soc.*, *80*, 1349–1361.

Blanford, H. F. (1884), On the connection of the Himalaya snowfall with dry winds and seasons of drought in India, *Proc. R. Soc. London*, *37*, 3–22.

Bonan, G. B. (1996), A land surface model (LSM version 1.0) for ecological, hydrological and atmospheric studies: Technical description and user's guide, *Tech. Note NCAR/TN-417+STR*, Natl. Cent. for Atmos. Res., Boulder, Colo.

Charney, J. G., and J. Shukla (1981), Predictability of monsoons, in *Monsoon Dynamics*, edited by J. Lighthill and R. P. Pearce, pp. 99–108, Cambridge Univ. Press, New York.

Chatterjee, P., and B. N. Goswami (2004), Structure, genesis and scale selection of the tropical quasi-biweekly mode, *Q. J. R. Meteorol. Soc.*, *130*, 1171–1194.

Chen, T.-C., and J.-M. Chen (1993), The 10–20-day mode of the 1979 Indian monsoon: Its relation with the time variation of monsoon rainfall, *Mon. Weather Rev.*, *121*, 2465–2482.

Cherchi, A., and A. Navarra (2003), Reproducibility and predictability of Asian summer monsoon in the ECHAM4-GCM, *Clim. Dyn.*, *20*, 365–379.

Fennessy, M., and J. Shukla (1994), Simulation and predictability of monsoons, in *Proceedings of the International Conference on Monsoon Variability and Prediction*, *WMO/TD 619*, pp. 567–575, Trieste.

Fennessy, M. J., and J. Shukla (1999), Impact of initial soil wetness on seasonal atmospheric prediction, *J. Clim.*, *12*, 3167–3180.

Ferranti, L., J. M. Slingo, T. N. Palmer, and B. J. Hoskins (1997), Relations between interannual and intraseasonal monsoon variability as diagnosed from amip integrations, *Q. J. R. Meteorol. Soc.*, *123*, 1323–1357.

Gadgil, S., and S. Sajani (1998), Monsoon precipitation in the AMIP runs, *Clim. Dyn.*, *14*, 659–689.

Gadgil, S., P. V. Joseph, and N. V. Joshi (1984), Ocean-atmospheric coupling over monsoonal regions, *Nature*, *312*, 141–143.

Goswami, B. N. (1994), Dynamical predictability of seasonal monsoon rainfall: Problems and prospects, *Proc. Indian Natl. Acad. Sci.*, *60A*, 101–120.

Goswami, B. N. (1998), Interannual variations of Indian summer monsoon in a gcm: External conditions versus internal feedbacks, *J. Clim.*, *11*, 501–522.

Goswami, B. N. (2005), South Asian monsoon, in *Intraseasonal Variability in the Atmosphere-Ocean Climate System*, edited by K. Lau and D. Waliser, pp. 19–61, Springer, New York.

Goswami, B. N., and R. S. Ajayamohan (2001), Intraseasonal oscillations and interannual variability of the Indian summer monsoon, *J. Clim.*, *14*, 1180–1198.

Goswami, B. N., V. Krishnamurthy, and H. Annamalai (1999), A broad-scale circulation index for interannual variability of the Indian summer monsoon, *Q. J. R. Meteorol. Soc.*, *125*, 611–633.

Goswami, P., and S. Srividya (1996), A novel neural network design for long-range prediction of rainfall pattern, *Curr. Sci.*, *70*, 447–457.

Gowarikar, V., V. Thapliyal, R. P. Sarker, G. S. Mandel, and D. R. Sikka (1989), Parametric and power regression models: New approach to long range forecasting of monsoon rain in India, *Mausam*, *40*, 125–130.

Hack, J. J. (1994), Parametrization of moist convection in the National Center for Atmospheric Research Community Climate Model (CCM2), *J. Geophys. Res.*, *99*, 5551–5568.

Hendon, H. H., and M. L. Salby (1999), The life cycle of the Madden-Julian oscillation, *J. Atmos. Sci.*, *51*, 2225–2237.

Holtslag, A. A. M., and B. A. Boville (1993), Local versus nonlocal boundary-layer diffusion in a global climate model, *J. Clim.*, *6*, 1825–1842.

Kalnay, E., et al. (1996), The NCEP/NCAR 40-year reanalysis project, *Bull. Am. Meteorol. Soc.*, *77*, 437–471.

Kang, I.-S., et al. (2002), Intercomparison of atmospheric GCM simulated anomalies associated with the 1997–98 El Nino, *J. Clim.*, *15*, 2791–2805.

Kang, I. S., J. Y. Lee, and C. K. Park (2004), Potential predictability of summer mean precipitation in a dynamical seasonal prediction system with systematic error correction, *J. Clim.*, *17*, 834–844.

Kiehl, J. T., J. J. Hack, G. B. Bonan, B. A. Boville, D. L. Williamson, and P. J. Rasch (1998), The National Center for Atmospheric Research Community Climate Model, *J. Clim.*, *11*, 1131–1150.

Kiladis, G. N., and M. Wheeler (1995), Horizontal and vertical structure of observed tropospheric equatorial rossby waves, *J. Geophys. Res.*, *100*, 22,981–22,997.

Kistler, R., et al. (2001), The NCEP NCAR 50-year reanalysis: Monthly means CD-ROM and documentation, *Bull. Am. Meteorol. Soc.*, *82*, 247–267.

Kriplani, R. H., and A. Kulkarni (1997), Climate impact of El Nino/La Nina on the Indian monsoon: A new perspective, *Weather*, *52*, 39–46.

Krishnamurthy, V., and B. N. Goswami (2000), Indian monsoon-ENSO relationship on interdecadal timescales, *J. Clim.*, *13*, 579–595.

Krishnamurthy, V., and J. Shukla (2000), Intraseasonal and interannual variability of rainfall over India, *J. Clim.*, *13*, 4366–4377.

Krishnamurti, T. (1985), Summer monsoon experiment - A review, *Mon. Weather Rev.*, *113*, 1590–1626.

Krishnamurti, T. N., and H. N. Bhalme (1976), Oscillations of monsoon system. Part I: Observational aspects, *J. Atmos. Sci.*, *45*, 1937–1954.
Krishnamurti, T. N., and D. Subrahmanyam (1982), The 30–50 day mode at 850 mb during monex, *J. Atmos. Sci.*, *39*, 2088–2095.
Krishnamurti, T. N., C. M. Kishtawal, T. E. LaRow, D. R. Bachiochi, Z. Zhang, C. E. Williford, S. Gadgil, and S. Surendran (1999), Improved weather and seasonal climate forecasts from multimodel superensemble, *Science*, *285*, 1548–1550.
Krishnamurti, T. N., C. Kishtawal, T. LaRow, D. Bachiochi, Z. Zhang, C. Williford, S. Gadgil, and S. Surendran (2000), Multimodel superensemble forecasts for weather and seasonal climate, *J. Clim.*, *13*, 4196–4216.
Krishnamurti, T. N., et al. (2001), Real-time multianalysis-multimodel superensemble forecasts of precipitation using trmm and SSM/I products, *Mon. Weather Rev.*, *129*, 2861–2883.
Krishnamurti, T. N., L. Stefanova, A. Chakraborty, T. S. V. V. Kumar, S. Cocke, D. Bachiochi, and B. Mackey (2002), Seasonal forecasts of precipitation anomalies for North American and Asian monsoons, *J. Meteorol. Soc. Jpn.*, *80*, 1415–1426.
Kumar, A., and M. P. Hoerling (1995), Prospects and limitations of atmospheric GCM climate predictions, *Bull. Am. Meteorol. Soc.*, *76*, 335–345.
Kumar, K. K., B. Rajagopalan, and M. A. Cane (1999), On the weakening relationship between the Indian monsoon and ENSO, *Science*, *284*, 2156–2159.
Lau, N. C. (1985), Modelling the seasonal dependence of atmospheric response to observed El Nino in 1962–76, *Mon. Weather Rev.*, *113*, 1970–1996.
Meehl, G. A., and J. Arblaster (1998), The Asian-Australian monsoon and El Nino-Southern Oscillation in the NCAR climate system model, *J. Clim.*, *11*, 1356–1385.
Nakazawa, T. (1986), Mean features of 30–60 day variations inferred from 8 year olr data, *J. Meteorol. Soc. Jpn.*, *64*, 777–786.
Numaguti, A. (1995), Characteristics of 4-to-20 day period disturbances observed in the equatorial Pacific during the TOGA COARE IOP, *J. Meteorol. Soc. Jpn.*, *73*, 353–377.
Palmer, T. N. (1994), Chaos and the predictability in forecasting monsoons, *Proc. Indian Natl. Acad. Sci.*, *60A*, 57–66.
Palmer, T. N., et al. (2004), Development of a European multimodel ensemble system for seasonal-to-interannual prediction (DEMETER), *Bull. Am. Meteorol. Soc.*, doi:10.1175/BAMS-85-6-853.
Ramanathan, V., and P. Downey (1986), A nonisothermal emissivity and absorptivity formulation for water vapor, *J. Geophys. Res.*, *91*, 8649–8666.
Reynolds, R. W., and T. M. Smith (1994), Improved global sea surface temperature analyses using optimum interpolation, *J. Clim.*, *7*, 929–948.
Sahai, A. K., A. M. Grimm, V. Satyan, and G. B. Pant (2003), Long-lead prediction of Indian summer monsoon rainfall from global SST evolution, *Clim. Dyn.*, *20*(7/8), 855–863.
Saji, N. H., and B. N. Goswami (1997), An intercomparison of the seasonal cycle of tropical surface stress simulated by 17 AMIP GCMs, *Clim. Dyn.*, *13*, 561–585.
Saji, N. H., B. N. Goswami, P. Vinayachandran, and T. Yamagata (1999), A dipole mode in the tropical Indian Ocean, *Nature*, *401*, 360–363.
Shukla, J. (1998), Predictability in the midst of chaos: A scientific basis for climate forecasting, *Science*, *282*, 728–731.
Shukla, J., and J. M. Wallace (1983), Numerical simulation of the atmospheric response to equatorial Pacific sea surface temperature anomalies, *J. Atmos. Sci.*, *40*, 1613–1630.
Sikka, D. R., and S. Gadgil (1980), On the maximum cloud zone and the ITCZ over Indian longitude during southwest monsoon, *Mon. Weather Rev.*, *108*, 1840–1853.
Sperber, K. R., and T. N. Palmer (1996), Interannual tropical rainfall variability in general circulation model simulations associated with atmospheric model intercomparison project, *J. Clim.*, *9*, 2727–2750.
Sperber, K. R., J. M. Slingo, and H. Annamalai (2000), Predictability and the relationship between subseasonal and interannual variability during the Asian summer monsoons, *Q. J. R. Meteorol. Soc.*, *126*, 2545–2574.
Walker, G. T. (1923), Correlation in seasonal variations of weather, iii: A preliminary study of world weather, *Mem. Indian Meteorol. Dep.*, *24*, 75–131.
Walker, G. T. (1924), Correlation in seasonal variations of weather. iv: A further study of world weather, *Mem. Indian Meteorol. Dep.*, *24*, 275–332.
Wang, B., R. Wu, and T. Li (2003), Atmosphere-warm ocean interaction and its impacts on Asian-Australian monsoon variation, *J. Clim.*, *16*, 1195–1211.
Wang, B., I.-S. Kang, and J.-Y. Lee (2004), Ensemble simulations of Asian-Australian monsoon variability by 11 AGCMs, *17*, 699–710.
Webster, P. J., V. O. Magana, T. N. Palmer, J. Shuka, R. T. Tomas, M. Yanai, and T. Yasunari (1998), Monsoons: Processes, predictability, and the prospects of prediction, *J. Geophys. Res.*, *103*(C7), 14,451–14,510.
Xie, P., and P. A. Arkin (1996), Analyses of global monthly precipitation using guage observations, satellite estimates and numerical predictions, *J. Clim.*, *9*, 840–858.
Yasunari, T. (1979), Cloudiness fluctuation associated with the northern hemisphere summer monsoon, *J. Meteorol. Soc. Jpn.*, *57*, 227–242.
Yasunari, T. (1980), A quasi-stationary appearance of 30–40 day period in the cloudiness fluctuation during summer monsoon over India, *J. Meteorol. Soc. Jpn.*, *58*, 225–229.
Zhang, G. J., and N. A. McFarlane (1995), Sensitivity of climate simulations to the parameterization of cumulus convection in the Canadian Climate Centre general circulation model, *Atmos. Ocean*, *33*, 407–446.

B. N. Goswami and P. K. Xavier, Centre for Atmospheric and Oceanic Sciences, Indian Institute of Science, Bangalore 560012, India. (goswamy@caos.iisc.ernet.in; xavier@caos.iisc.ernet.in)